Progress in Disaster Science 13 (2022) 100212

Contents lists available at ScienceDirect

Progress in Disaster Science

journal homepage: www.elsevier.com/locate/pdisas

Investigating major causes of extreme floods using global datasets: A case of Nepal, USA & Thailand

N. Shalinda Fernando [a,b], Sangam Shrestha [a,c,*], Saurav KC [a], S. Mohanasundaram [a]

[a] School of Engineering and Technology, Asian Institute of Technology, P.O. Box 4, Klong Luang, Pathum Thani 12120, Thailand
[b] Regional Integrated Multi-Hazard Early Warning System (RIMES) for Africa and Asia, Outreach Building, Asian Institute of Technology Campus, Klong Luang, Pathum Thani, Thailand
[c] Stockholm Environment Institute, Asia Center, Chulalongkorn Soi 64, Phayathai Road, Pathumwan, Bangkok 1033, Thailand

ARTICLE INFO

Article history:
Received 10 August 2021
Received in revised form 27 December 2021
Accepted 30 December 2021
Available online 3 January 2022

Keywords:
Flood driver
PERSIANN
ESACCI-LC
Multiple linear regression

ABSTRACT

In recent years, the damages caused by flooding has been severe globally, and several research studies indicated extreme precipitations and changes in land-use plays a crucial role. The hydrological and climate impact studies in data-scarce regions are relatively challenging, and several global dataset products have aided in overcoming them. However, their accuracy and reliability vary from climatic regions to the topography of the land surface. Therefore, this study employed global dataset products for precipitation and land use to identify the major flood driver in tropical, subtropical, and temperate regions where severe flooding had occurred in the past decade. The study evaluated the performances of the PERSIANN-CDR, PERSIANN-CCS and PERSIANN precipitation products, and ESACCI-LC land-use product to develop a statistical relationship among the land-use and extreme precipitation variables using the Multiple Linear Regression technique. The result shows that the PERSIANN-CDR estimates were more accurate than others in the selected study basins. The statistical model showed that the combined contribution of both land-use and precipitation to the flood (R^2) are 73.9%, 66.7% and 37.4%, for the Mun River Basin (MRB), Thailand, the Bagmati River Basin (BRB), Nepal and the Missouri Little Sioux (MLSB) Basin, USA, respectively. Moreover, it correlated with the flood (R) by 85.9%, 81.7% and 61.1% in the MRB, BRB, and MLSB, respectively. Additionally, the results indicated that the major cause of flooding in MRB and BRB is likely to be the changes in precipitation, while land-use change is likely to be the major cause in the MLSB. The result from the study shall be useful for the researchers, practitioners, and decision-makers in determining the applicability of a suitable precipitation product in data-scarce regions, visualise the major cause of flooding and plan the flood risk management strategies accordingly by minimising the exposure and maximising the resiliency for possible future events.

1. Introduction

Flooding accounts for one of the various natural disasters for which the damages it causes are innumerable. This phenomenon occurs in varying duration at different intervals. As a result, it causes severe harm to several sectors such as transportation, economy, environmental ecosystem, cultural heritage sites, and most importantly human lives [46]. Pradhan [56] mentioned that more than 33% of the land area in the world is susceptible to flood. In 2011, hydrological disasters accounted for 52% of natural disasters that affected 140 million people with 20.4% resulting in deaths, and a total of 19.3% resulting in damages, and with a total economic loss of $US 70.1 billion worldwide [25]. As a result, economic losses due to flooding events are usually millions of dollars each year [70]. It was also noted that according to Guha-Sapir et al. [25] that during 2011, the brought about losses from flooding covered 40% of all-natural disasters. Researchers and scientists have found that key drivers of floods tend to be both natural and anthropogenic factors such as climate change, deforestation, increasing population, environmental degradation, and intensified land-use. Thus, the effect of flooding restricts the sustainable development of economies and societies [28].

Nowadays, the main justification for escalating flood losses is due to insufficient studies conducted and the data scarcity in flood vulnerable areas, and lack of an adequate precautionary plan to prevent the losses from a flood [41]. To address this issue, Global Precipitation Products (GPP) were developed and can be classified into gauge-based products, satellite-based precipitation estimates and reanalysis datasets as mentioned on Sun et al. [66]. New studies have immersed on the performance of the satellite-based precipitation estimates (SPE) as a method of measuring precipitation and enhancement of forecasts [61]. Also, SPE products are widely made use of in understanding and investigating of extreme phenomena's

* Corresponding author at: School of Engineering and Technology, Asian Institute of Technology, P.O. Box 4, Klong Luang, Pathum Thani 12120, Thailand.
E-mail address: sangam@ait.asia (S. Shrestha).

http://dx.doi.org/10.1016/j.pdisas.2021.100212

such as drought and flooding events that have reported an escalating upward trend globally [62].

A few examples of extensively used SPEs are the Precipitation Estimation from Remotely Sensed Information using Artificial Neural Networks (PERSIANN) family of products [5,29,62], Tropical Rainfall Measuring Mission (TRMM) [34] and Global Precipitation Climatology Project (GPCP) [1]. The precision and reliability of the SPEs depends on the catchment size, basin topography, precipitation mechanism, precipitation type and climates of various regions and their seasons [66]. Khan et al. [39] utilized the SPE products as an input for precipitation in river basins comprising complex physiographical characteristics for replicating the streamflow and advised that no single SPE product is capable of robust performance in the global context. Furthermore, it was demonstrated that the accuracy and precision of the SPE products are solely based on their type of application. In recent years, precipitation products of the PERSIANN family have been utilized regularly for various hydrological applications such as evaluation against observed gauged-records, other global precipitation products and model simulations [45,47,49,76], runoff prediction [9,30], drought monitoring [2,38], rainfall frequency analysis [23] and modelling soil moisture [37].

Land-use change and floods are strongly correlated; thus, major alterations in land-use and land cover (LULC), such as a watershed faced with rapid urbanization, would generate a series of flood occurrences thereby resulting in more human and economic loss. For effective management of natural resources, information regarding LULC and their variations remain vital and are indeed pre-requisites for assessment [3]. Thus, the main source of monitoring the global landscape is by utilizing global land cover dataset products. A few examples of the global land-use products are GLC 2000 [8], MODIS [22] and ESACCI-LC [17]. Recent studies reported by Mousivand and Arsanjani [48]; Pérez-Hoyos et al. [54] and Chirachawala et al. [12] had supported the applicability of the ESACCI-LC datasets for monitoring global landscapes.

Costa et al. [14] had also proven that an increase in urban built-up, intensive annual cropping, and areas that are under heavy grazing pressure led to changes in the hydrological regime. For many centuries, the forests had been believed to safeguard against flooding therefore it intrigued researchers on the examination of the trade-off. In past studies, various statistical techniques were adopted by Bradshaw et al. [10] and Ferreira and Ghimire [19] demonstrated that forest trends are important to flood dynamics and that loss of forests will have a probable increase in future flood-related catastrophes. Thus, the main goal of this research was to investigate the major attribute between precipitation and land-use change, for recent severe floods by adopting global dataset products. Hence, this study paves the way for forthcoming research prospects of GPPs by evaluating the PERSIANN family of products in the selected study basins and more importantly, investigating the main attribute of the flood event by establishing a statistical relationship.

2. Materials and methods

2.1. Study area

For this research, the study basin selection was based upon the data which was acquired from the Dartmouth Flood Observatory (DFO) and can be retrieved from https://floodobservatory.colorado.edu/Archives/index.html. The selection criteria of the study basins were constructed for the occurrence of very large or extreme fluvial flooding (explained by indices on DFO) during the recent past decade (2010 – 2020) in 3 independent climatic regions where there was no influence of a major flood control reservoir.

In Nepal, during July 2019, the monsoon rain brought forth flooding and landslides that damaged numerous infrastructures. Apart from that, dozens of households were reported dead or missing while hundreds were displaced in several districts of Nepal, mainly in the capital, Kathmandu. It was disclosed that four rivers across Nepal were reported to water levels of above danger level, the Bagmati river was revealed as one of these rivers. [20].

In the United States, the 2019 Mid-western floods had affected a total area of 492,797.4km^2. Several states such as Nebraska, Iowa, Wisconsin, Missouri, Kansas, Illinois, Minnesota and South Dakota. The extent of total economic damage caused due to this flood was US$ 4 billion of which Iowa contributed US$ 1.6 billion [21].

In Thailand, during October 2010, according to the Mueang Nakhon Ratchasima District Office, the flood caused physical damage to 16 Government units, 13 hospitals, 2 reservoirs and 24,785 households were displaced [52]. Table 1 illustrates the summary of flooding events. Here, the flood magnitude scale represents the flood run-off volume to the flood of record where 10 represents the maximum (flood of record) and 0 represents the minimum. SI = 1.5 explains significant damage has been caused and is greater than 2 decades but less than a 100-year return period since the last similar event (affecting >5000 sq. km), SI = 2 explains the damage caused is estimated for a recurrence period greater than 100 years.

The above-stated flood losses and damages have occurred and affected the study basins shown in Fig. 1. These three river basins experience different climate patterns as they are located in the sub-tropical, temperate and tropical climate regions. There are also several climatic and physiographical differences among the selected study basins, such as the different ranges of altitude in the catchments, different shape, size and catchment area of the watershed, diverse quantities of various land cover types in the catchments and the spatio-temporal variability of annual rainfall and annual streamflow across selected river basins. Hence, this study employed a holistic approach to identifying the major flood attribute between precipitation and land-use, for these independent river basins which have confronted and experienced extreme flooding. See Table 1 for detailed attributes of the flood events of the three regions of interest.

2.1.1. Bagmati River basin, Nepal

This Bagmati River Basin (BRB) is located within 26°45′ – 27°49′ north latitudes and 85°02′ – 85°57′ east longitudes in the southern central part of Nepal as shown in Fig. 1 (a). The basin covers an area of nearly 3420 km^2 within Nepal and is dominated mainly by forest cover (57%). The basin has a population of 2.3 million according to 2001 census data and receives an annual rainfall of 1800 mm [6]. The main seasons which are associated with the BRB are Winter (Dec. to Feb.), Spring (Mar. to May), Summer (Jun. to Sept.), and Autumn (Oct. and Nov.) [60].

The Pandheradovan hydrological station is located at 27.10°N and 85.475°E which is at the lower part of the basin. The maximum annual discharge of the basin is 1219 MCM in July and the minimum annual discharge is 38.11MCM in March and a mean annual discharge of 331 MCM.

2.1.2. Missouri-Little Sioux Basin, USA

The Missouri-Little Sioux basin (MLSB) is located at an intersection of Iowa, South Dakota, and Nebraska (41° 3′- 43° 41′ north latitude and 96° 42′ - 94° 50′ west longitude). Fig. 1 (b) shows the basin map of the sub-

Table 1
Summary of case studies on extreme flooding (Source: DFO).

Country	Lat (°)	Lon (°)	Start of Flooding	End of Flooding	TEL (US $)	Fatalities	TAA (km^2)	FM Scale	SI Class
Nepal	27.69	84.15	08/07/2019	15/07/2019	N. A	119	87,390.9	6.02	1.5
USA	40.28	−94.50	12/03/2019	28/03/2019	1.6 bil.	3	492,797.4	7.22	2
Thailand	15.03	102.20	10/10/2010	15/11/2010	2.3 bil.	206	3873.76	5.46	2

FM: Flood Magnitude, SI: Severity Index, TAA: Total Area Affected, TEL: Total Economic Loss.

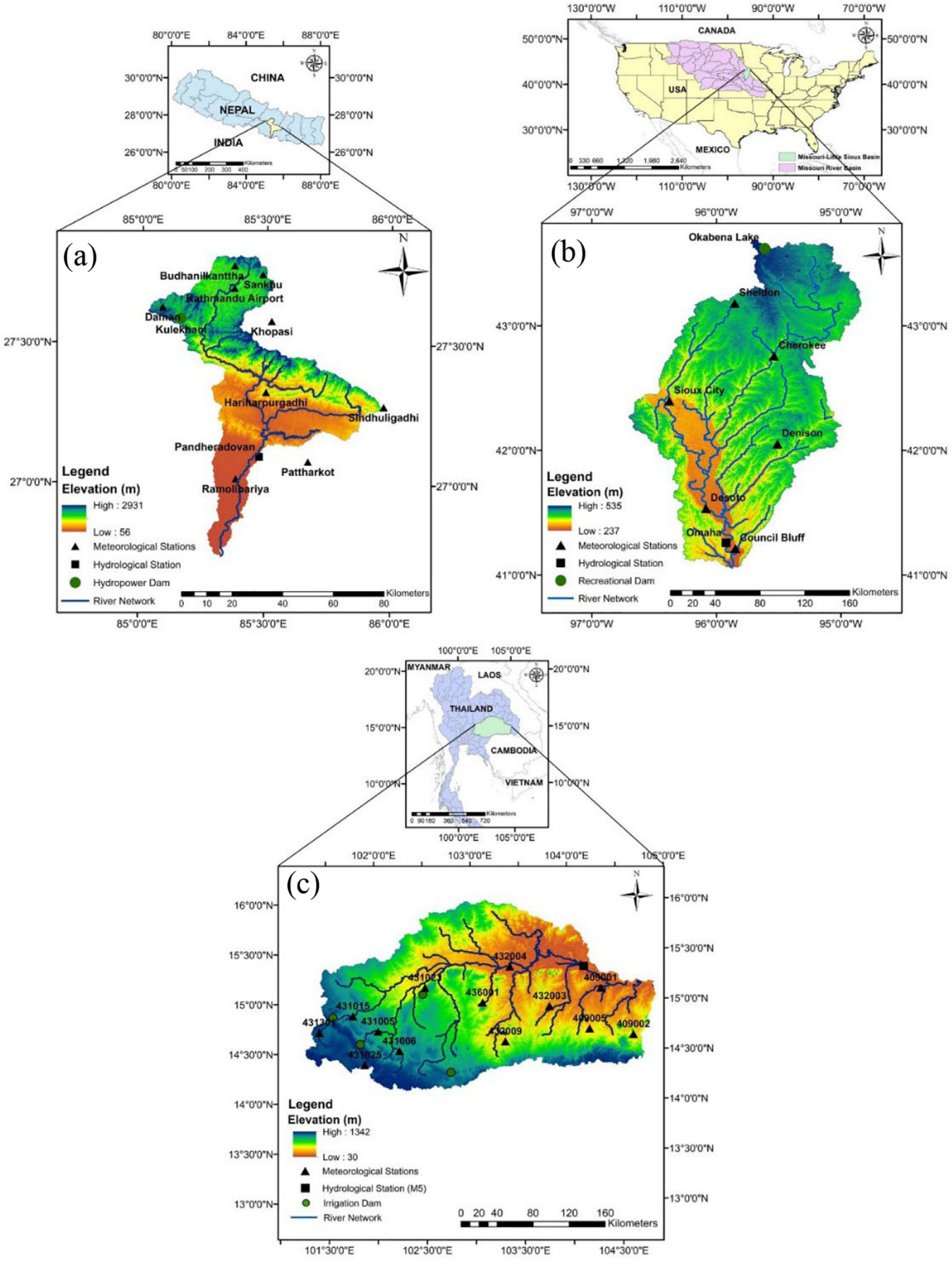

Fig. 1. Location map of selected study basins (a) Bagmati River Basin, Nepal, (b) Missouri-Little Sioux Basin, USA and (c) Mun River Basin, Thailand with meteorological and hydrological stations, dam, and river network.

watershed MLSB (24,156.9 km^2) of the major basin, the Missouri River Basin which drains a total area of 1.37 million km^2. The basin is dominated by Cropland which accounts for 86% of its basin area. The elevation in the basin ranges from 237 masl to 535 masl. The annual precipitation in the region averages around 863.6 mm, more specifically in the Iowa state, precipitation ranges from as low as 660.4 mm in the northwest to as high as 965.2 mm when circulating towards the southeast region.

The main seasons which are experienced in the MLSB are Winter (Dec. to Feb.), Spring (Mar. to May), Summer (Jun. to Aug.), and Autumn (Sept. to Nov.). The Little Sioux River Watershed has less rangeland and more channelization due to more intensive crop farming [53]. The temperatures during the summer are optimal for soybean and corn growth, yet, not so extreme in magnitudes as to cause severe crop stress. Furthermore, the crops are able to have an optimal dry-down during the fall months and are readily accessible for harvesting. It should also be noted that the soils are frozen beginning early December till late March as a result of the cold winters [27]. The Omaha hydrological station is located at 41.26°N and 95.92°W which is at the lower part of the catchment. The maximum annual discharge of the basin is 3779.1 MCM in July and the minimum annual discharge is 1593.07 MCM in February and a mean annual discharge of 2814.5 MCM.

2.1.3. Mun River basin, Thailand

The Mun River Basin (MRB) located in the north-east of Thailand (14°–16° N and 101° 30′–105° 30′E) supports the total population of 13,576,828. The basin has a total catchment area of 71,060km^2 covering ten provinces. The MRB experiences generally a Savanna Climate which is generally humid, hot, and dry weather. It is also observed that almost 70% of the watershed is used for agricultural purposes. The Mun River is a tributary of the Mekong River, as it originates near the Nakhon Ratchasima Province and joins the Mekong River at the Ubon Ratchathani Province [75].

Namely, Lower Mun (LM), Middle Mun (MM) and Upper Mun (UM), comprising catchment areas of 17,439 km^2, 30,308 km^2, and 23,313 km^2 respectively. However, since there was a major reservoir (Sirindhorn reservoir) present in the Lower Mun basin, this study considered only UM and MM catchments for analysis. The M5 hydrological station is located at 15.34°N and 104.15°E which is in the eastern region of the catchment. The maximum annual discharge of the basin is 2261.95 MCM in October and the minimum annual discharge is 14.29 MCM in March and a mean annual discharge of 576.3 MCM. Fig. 1 **(c)** shows the UM and MM catchments of the MRB.

2.2. Data collection

Table 2 lists the summary of data acquisition for precipitation, land-use, topography and streamflow used in this study. As on-site precipitation data was not available for the Missouri-Little Sioux basin, USA, it was examined with the GPCC Full Data Daily V.2018 product which provides 1.0° spatial resolution gauged-gridded rainfall data [78]. This dataset consists of rainfall data provided from the national hydrological and meteorological services, global and regional data collections and the data from the World Meteorological Organization - GTS (Global Telecommunication System).

2.2.1. PERSIANN precipitation products

During the past two decades, the Centre for Hydrometeorology and Remote Sensing (CHRS) at the University of California, Irvine, in collaboration with the National Oceanic and Atmospheric Administration (NOAA), National Aeronautics and Space Administration (NASA), and United Nations Educational, Scientific and Cultural Organization (UNESCO) program has developed the PERSIANN precipitation products. The available products are, namely, PERSIANN, PERSIANN-CCS and PERSIANN-CDR, hereafter referred to as PERSIANN, CCS and CDR, respectively. These products are publicly available and can be accessed via https://chrsdata.eng.uci.edu/. These spatial coverage of all three products are available in the latitude band range of 60^{0}S – 60^{0}N. The shortest temporal frequency available for CDR data is in daily frequency and consists of a dataset length of nearly 38 years. Hence, CDR is suitable for assessing the statistical trends of hydro-met phenomena. Contrastingly, the shortest temporal frequency available for both CCS and PERSIANN is in hourly frequency, as they are targeted to assist in decision-making processes. CCS is more suitable for monitoring the formation of hurricanes as it is accessible in real-time (1-h lag) whereas PERSIANN has a time delay of two-days as it prioritises to represent quality controlled data [50]. The various sources and techniques of data retrieval and information on ANN routines of each PERSIANN family product are stated as follows.

In 1997, the ANN routine of the PERSIANN product is constructed on the symbiosis among the high-frequency samples from GEO (Geostationary earth orbiting) satellites and the sampled information from LEO (Low earth orbiting) satellites [62]. The routine of the ANN model is known as Modified Counter Propagation and is based on the multilayer neural feedforward network (MFN). The PERSIANN algorithm originally utilized the longwave infrared retrievals as the main input. Despite that, advances to the algorithm were made via the inclusion of daytime visible imagery. The ANN model is based on PMW (Passive Microwave) rainfall originating out from LEO satellites and is employed for updating the ANN routine via the processes of hidden out and input hidden transformations. Most importantly, the estimation of parameters for each progression can be accomplished individually through a supervised learning strategy for the latter while the training model is employed for the former [31–33,62,63]. The PERSIANN data is available from March 2000 till the present.

PERSIANN–Cloud Classification System (PERSIANN-CCS) is based upon the cloud-patch-based algorithm where cloud coverage features are extracted under specified temperature thresholds. The ANN routine of the CCS works with greater infrared cloud imagery compared to PERSIANN by segmenting cloud images under different temperature thresholds. Then, the features (geometry, texture, and temperature) are retrieved from the images that have been segmented. Succeeding, the extracted cloud features are classified into distinct categories via the SOFM (self-organizing feature map) clustering algorithm. Lastly, a relationship was developed for each feature between rainfall rate and brightness temperature using histogram matching and non-linear exponential function fitting [29]. The CCS data is available from January 2003 till the present.

PERSIANN–Climate Data Record (PERSIANN-CDR) provides rainfall estimations since 1983. The ANN algorithm of CDR uses inputs from infrared imagery via different sources of international GEO satellites. These satellites are under the International Satellite Cloud Climatological Project (ISCCP) which are managed by the NOAA. This product further trains the ANN routine model by incorporating the data from the National Centers for Environmental Prediction (NCEP) Stage IV hourly precipitation. Moreover, to reduce the bias of the precipitation estimates, the PERSIANN-CDR product is processed with the Global Precipitation Climatology Project (GPCP) monthly 2.5° precipitation data, such that consistency is maintained [5].

2.2.2. ESACCI land cover product

The United Nations (UN) Food and Agricultural Organization (FAO) developed the European Space Agency Climate Change Initiative (ESACCI). The ESACCI produced a time series of global land cover at a 300-m spatial resolution covering an annual time step temporal span from 1992 to 2015. It can be retrieved from https://www.esa-landcover-cci.org/. The land cover changes are detected at 1 km based on satellites such as the AVHRR time series between 1992 and 1999, SPOT-VGT time series between 1993 and 2013, and PROBA-V time series for 2013, 2014, and 2015. When the MERIS FR time series are available, the detected map at 1 km is remapped to 300 m of resolution [17].

For LU change analysis, the extracted land cover data were reclassified into nine distinct LU classes using ArcMap 10.1 that were common for all years (1992–2015). The nine major classes are defined as follows: (1) Cropland (i.e., Rainfed trees, shrubs), (2) Natural vegetation (Mosaic croplands) (3) Forest (i.e., evergreen forest, deciduous forest), (4) Urban built-up (i.e., city, commercial and services, industries, etc.), (5) Water bodies (i.e., rivers, reservoirs, irrigation canals, ponds), (6) Grasslands

Table 2
Data acquired for this study.

SI no.	Type of Data/Name of Dataset	Temporal Span	Temporal Frequency	Spatial Resolution	Data Source
1	*Precipitation*				
	PERSIANN-CDR	1993–2018	Daily	$0.25^0 \times 0.25^0$ (28 km × 28 km)	
	PERSIANN-CCS	2003–2018	Daily	$0.04^0 \times 0.04^0$ (4 km × 4 km)	https://chrsdata.eng.uci.edu/
	PERSIANN	2000–2018	Daily	$0.25^0 \times 0.25^0$ (28 km × 28 km)	
	GPCC Full Data Daily Version.2018	1993–2015	Daily	$1.0^0 \times 1.0^0$ (111 km ×111km)	https://opendata.dwd.de/climate_environment/GPCC/full_data_daily_V2018/
2	*Land-use*				
	ESACCI-LC	1992–2015	Annual	300 m × 300 m	https://www.esa-landcover-cci.org/.
3	*Topography*				
	ASTER GDEM 003	2000–2013	–	30 m × 30 m	https://lpdaac.usgs.gov/products/astgtmv003/
4	*Streamflow*				
	GRDC	1993–2018	Daily	–	https://portal.grdc.bafg.de/
	Observed Data -RID	1996–2015	Daily	–	Royal Irrigation Department, Thailand
	Observed Data -DHM	1993–2010	Daily	–	Department of Hydrology and Meteorology, Nepal

(i.e., herbaceous cover), (7) Shrublands (8) Wetlands and (9) Bare Areas. However, some basins analyzed in this study do not have all 9 classes as there is no presence of the land-use type as defined in the major land-use classes. All land cover (LC) maps were projected into a common coordinate system (UTM) prior to the image analysis.

2.2.3. GRDC

The Global Runoff Database at Global Runoff Data Centre (GRDC) has global river discharges of 160 countries covering over 9000 stations. This unique dataset comprises data at daily or monthly time steps. The World Meteorological Organization (WMO) manages and operates the GRDC and assists research on investigating the trends of global climate. Thus, it enables scientists to utilize the GRDC facilities for research projects [64]. This data can be retrieved from https://portal.grdc.bafg.de/.

2.3. Methodology

The GPPs employed in this research was selected based upon the spatio-temporal performances and common applications used in the global context. The GPPs were collected in Network Common Data form (NetCDF) and were extracted into Comma Separated Values (CSV) format by utilizing RStudio. As illustrated in Fig. 2**.** Initially, the GPPs were validated and evaluated with rain gauge records via detection metrics and statistical indicators using the point to pixel method, where the point refers to the rain

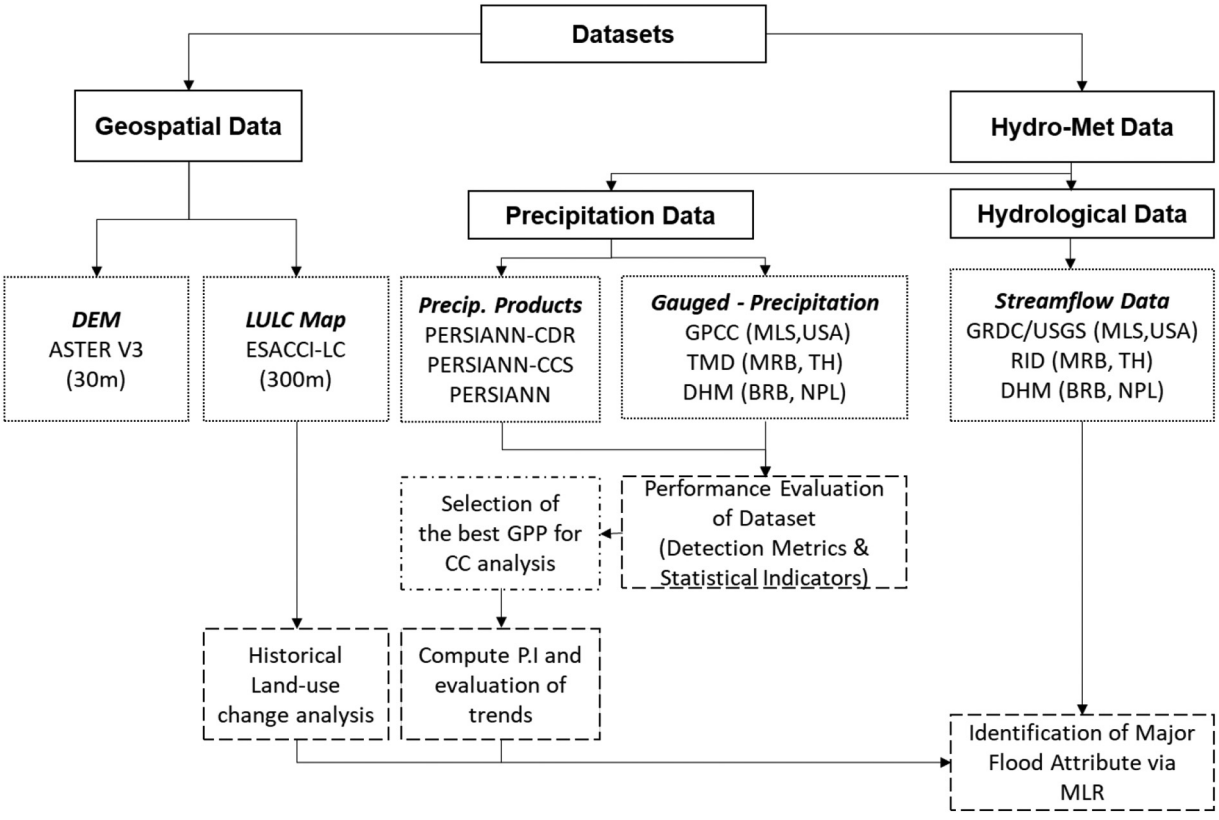

Fig. 2. Overall research framework.

gauge and the pixel refers to the GPP's gridded data. Gunathilake et al. [26] had adopted a similar approach to validate GPPs to observed rain gauge records (stations that fall under the same grid were considered as one). Followed by the evaluation and assessment of trends in the extreme precipitation indices of the study basins. Succeeding, the historical land-use change analysis was conducted in the study basins. Finally, a statistical relationship was established to observe the contributions between precipitation and land-use change to flooding in the selected basins.

2.3.1. Performance evaluation indicators of global precipitation products

Before the analysis, it is noteworthy to mention that, the three PERSIANN products lack rainfall data in few intervals due to the input geostationary satellites undergoing maintenance hence, the unavailability. Therefore, the missing rainfall data of the GPPs were fulfilled using the arithmetic average technique if the missing rainfall data was less than 10%, however, if the missing rainfall data was greater than 10%, the normal ratio method was utilized for fulfilling the missing rainfall data [65]. The capability of observed rainfall detection of GPPs was assessed via the Probability of Detection (POD), the Critical Success Index (CSI) and the False Alarm Ratio (FAR). These indicators have been similarly used by Gunathilake et al. [26] for evaluating GPPs. POD refers to the likelihood of detecting the rainfall, the CSI explains the success rating of estimating the rainfall event whereas, FAR represents the false fraction of the satellite diagnosed events. The notions of hits, misses, false alarms, and correct negatives are described in Supplementary Table S1.

$$POD = \frac{(hits)}{(hits + misses)} \tag{1}$$

$$CSI = \frac{(hits)}{(hits + misses + false\ alarms)} \tag{2}$$

$$FAR = \frac{(false\ alarms)}{(hits + false\ alarms)} \tag{3}$$

The accuracy and precision of rainfall estimation by the satellite products were measured by root mean square error (RMSE) and the Pearson's correlation (r).

$$RMSE = \sqrt{\frac{\sum_{i=1}^{n} (y_i - x_i)^2}{n}} \tag{4}$$

$$r = \frac{n\sum xy - (\sum x)(\sum y)}{\sqrt{n\sum x^2 - (\sum x)^2} \times \sqrt{n\sum y^2 - (\sum y)^2}} \tag{5}$$

where y_i represents the estimate of the GPP (in mm), x_i represents the observed rainfall (in mm) and n represents the number of samples.

2.3.2. Computation of extreme precipitation indices

Extreme precipitation indices were computed using RClimDex 1.0 to identify the attributes and trends of rainfall patterns during the study period [77]. Precipitation indices were computed at a 5% significance level in the selected study basins. The indices considered were, namely, R10 (No. of days >10 mm), R20 (No. of days >20 mm), R35 (No. of days >35 mm), CWD (Maximum no. of consecutive days >1 mm), R95p (Annual rainfall >95th percentile rainfall), R99p (Annual rainfall >99th percentile rainfall) and PRCPTOT (Annual rainfall in wet days ≥ 1 mm). Strengths in the trends are classified as, Very Strong (VS; $0 < p \leq 0.01$), Strong (S; $0.01 < p \leq 0.05$), Weak (W; $0.01 < p \leq 0.05$), Little (L; $0.10 < p \leq 0.50$) and Very Little (VL; $0.50 < p \leq 1.0$) as similarly classified in Khattak et al. [40]. The magnitude and direction of the trends of the precipitation indices were computed using the Mann-Kendall trend test [79] and Sen's slope estimator [80] similarly as in Khattak et al. [40].

2.3.3. Multiple linear regression

Multiple Linear Regression (MLR) was used to assess the contribution of each flood driver by establishing a statistical relationship among the flood and land-use change and the extreme precipitation indices of the study basins.

This study considers the Annual Peak Flow (APF) which is defined as the maximum mean daily streamflow as the dependant variable while the independent variables are the extreme precipitation indices and land-use change. Contreras et al. [13] used similar predictor variables such as Global Climate Indices and LULC percentages to explain the streamflow variability. Three statistical models were computed for LU, precipitation, and the combination of LU and precipitation using the SPSS tool at a confidence level of 95% to assess the contribution of each predictor by the coefficient of determination (R^2).

The samples size varied from each basin as data was not available in the same temporal span. Despite that, the sample size of each basin fulfilled the minimum criteria ($n = 10$) recommended by VanVoorhis and Morgan [73]. Kutner et al. [42] stated that predictor variables that may correlate among themselves do not, inhibit the ability to obtain a good fit nor does it affect to mean responses of new observations. The residual autocorrelation was determined by the Durbin-Watson (DW) test. The values of the DW test vary from 0 to 4. Generally, a value close to 2 is regarded as free of autocorrelation at a certain significance level [11]. Glen [24] recommends that test statistic values in the range of 1.5 to 2.5 are relatively normal, values outside of this range could be cause for concern.

3. Results and discussion

3.1. Performance of global precipitation products

In terms of the data coverage of the GPPs, the CDR estimates had 99.70%, 99.62% and 99.69% coverage in the BRB, MLSB, MRB, respectively. The CCS estimates provided 99.95%, 99.98% and 99.92% data coverage for the BRB, MLSB, MRB, respectively. While, the PERSIANN estimates exhibited 98.98%, 99.02% and 98.99% data coverage in the BRB, MLSB, MRB, respectively. Therefore, as the percentage of missing data was less than 10%, the missing data was fulfilled through the arithmetic average technique.

The estimates of the GPPs of the Bagmati River basin, Nepal, and Mun River basin, Thailand are examined with corresponding data from the Department of Hydrology and Meteorology (DHM), Nepal, and the Thai Meteorological Department (TMD), Thailand, respectively. While the estimates of the Missouri-Little Sioux basin, USA are examined with the GPCC dataset. Fig. 3. illustrates the summary of the results through detection metrics of the GPPs in the study basins.

In terms of capturing the observed rainfall events, the CDR performed well in all study basins as they generated high POD values when in comparison to other products. The best values were recorded for CSI with the CDR product in all study basins. In terms of FAR results, the PERSIANN product performed well in the BRB while the CCS produced the best performance in both MLSB and MRB. Fig. 4. illustrates the summary of the correlation results of the GPPs. Fig. 5. displays the summary of the RMSE results of the GPPs.

In the BRB, the GPPs were evaluated for the 'Sankhu' and 'Hariharpurgadhi' stations which are at an elevation of 1449 m and 250 m, respectively. Observed rainfall data for the Sankhu was available from 1993 to 2011 while observed rainfall data for Hariharpurgadhi was available from 1993 to 2009. It was clear that all GPPs had underestimated the precipitation in both stations. PERSIANN-CDR had produced the lowest RMSE in both monthly and annual temporal scales in both stations of high and low elevations. At Sankhu, monthly estimated correlations were 0.78, 0.74 and 0.60 with RMSE values of 163.58 $mmmon^{-1}$, 169.52 $mmmon^{-1}$ and 171.66 $mmmon^{-1}$ for CDR, CCS and PERSIANN, respectively. Whereas annual estimates had correlations of 0.36, 0.62 and 0.59 with RMSE values of 941.87 $mmyr^{-1}$, 1093.82 $mmyr^{-1}$ and 1340.94 $mmyr^{-1}$ for CDR, CCS and PERSIANN, respectively. For Hariharpurgadhi,

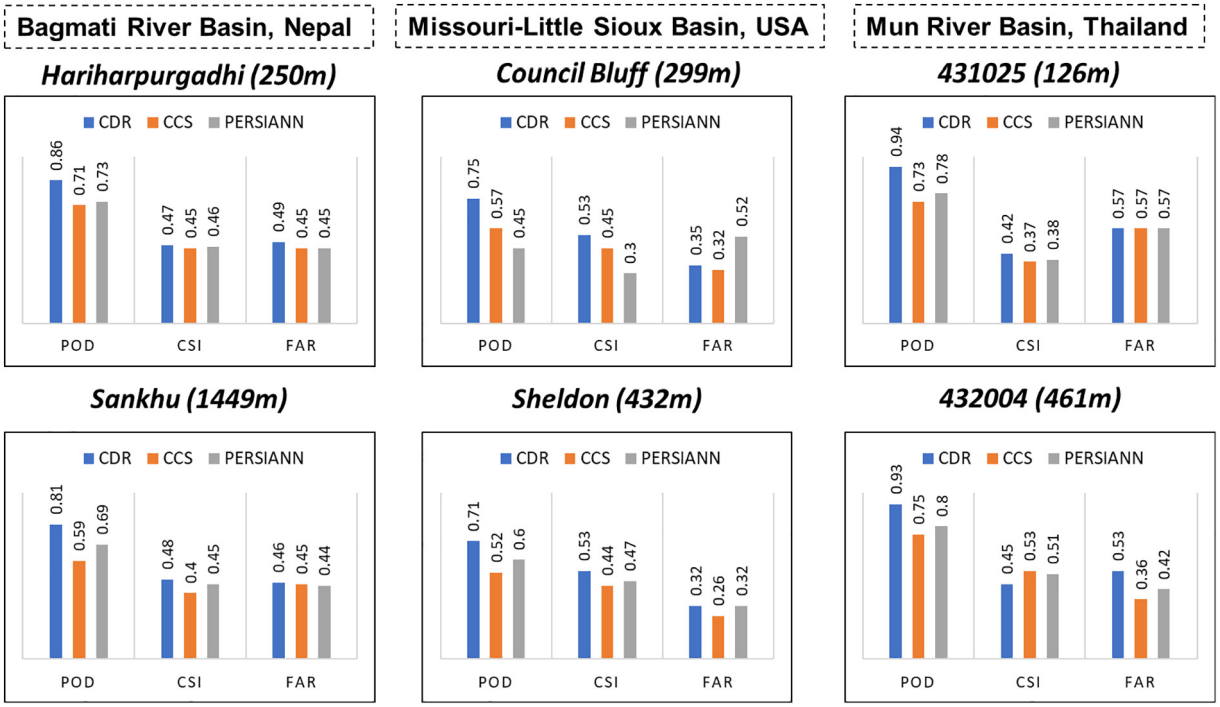

Fig. 3. Results of Detection Metrics of Study Basins.

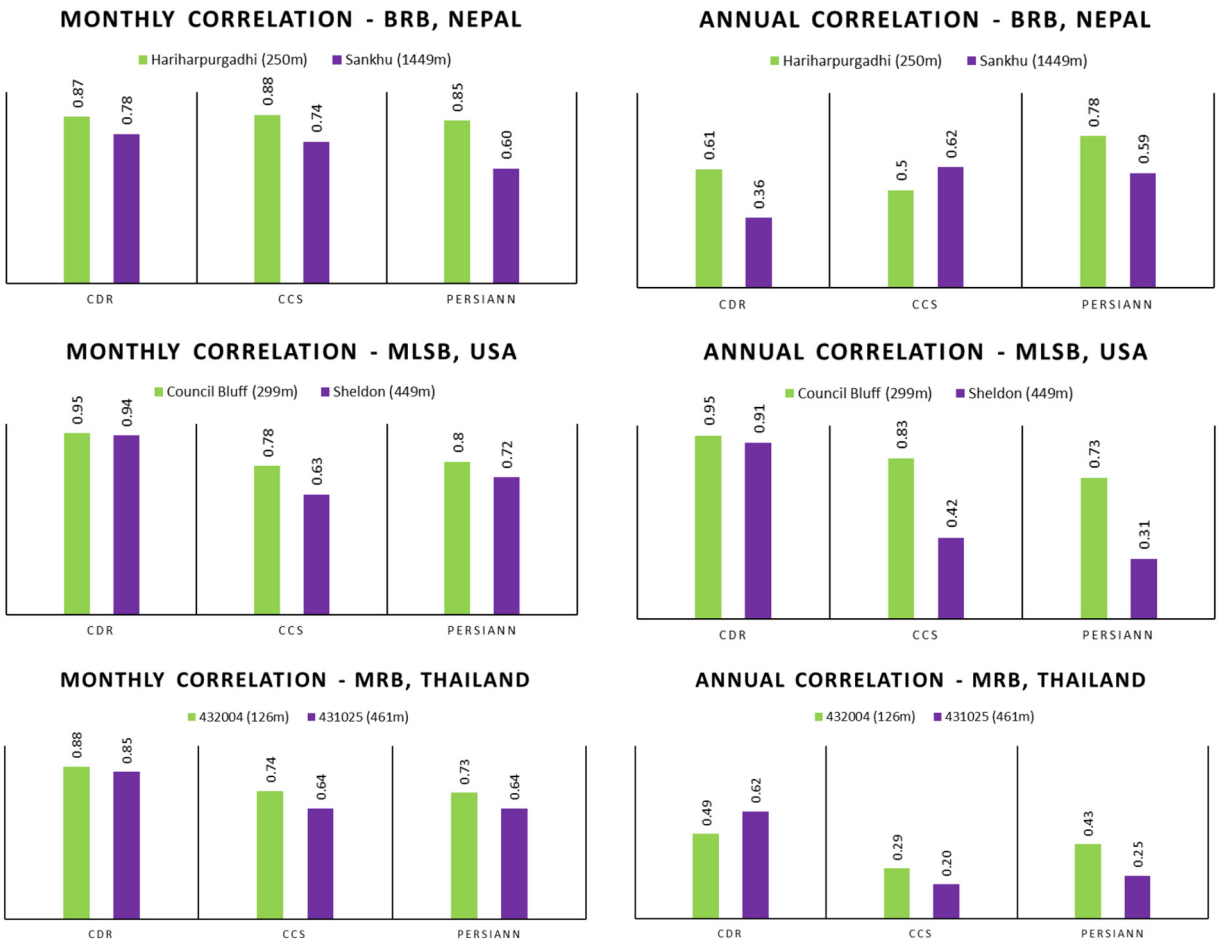

Fig. 4. Results of Monthly and Annual Correlation Analysis in Study Basins.

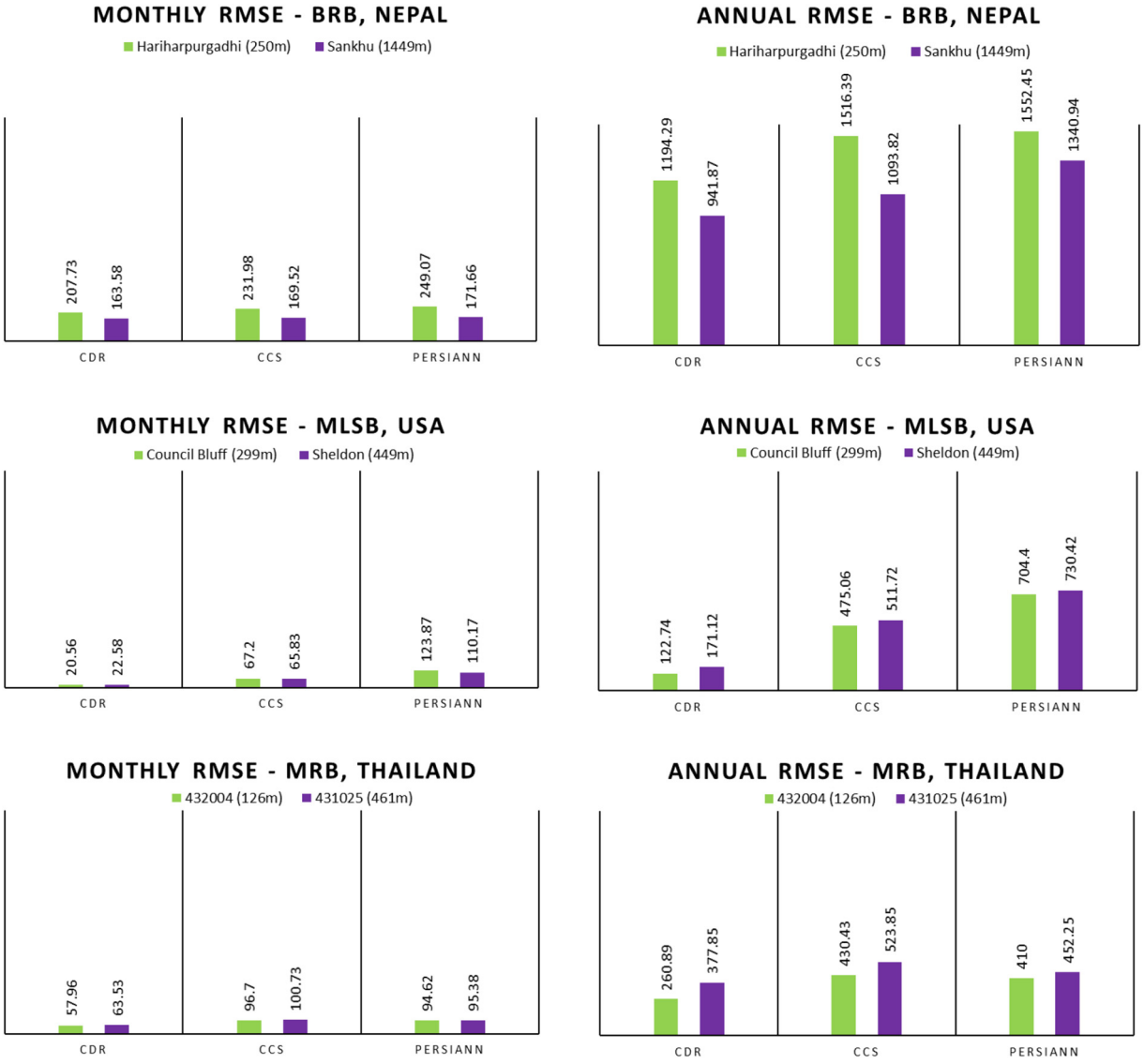

Fig. 5. Results of Monthly and Annual RMSE Analysis in Study Basins.

monthly estimated correlations were 0.87, 0.88 and 0.85 with RMSE values of 207.73 $mmmon^{-1}$,231.98 $mmmon^{-1}$ and 249.07 $mmmon^{-1}$ for CDR, CCS and PERSIANN, respectively. Whereas annual estimated correlations were 0.61, 0.50 and 0.78 with RMSE values of 1194.29 $mmyr^{-1}$, 1516.39 $mmyr^{-1}$ and 1552.45 $mmyr^{-1}$ for CDR, CCS and PERSIANN datasets, respectively.

In the MLSB, the GPPs were evaluated for the 'Council Bluff' station and 'Sheldon' station which is located at an elevation of 299 m and 449 m. Observed rainfall data for both stations were available from 1993 to 2015. In general, it was noted that the GPPs had overestimated the precipitation with the PERSIANN product having the largest overestimation. For Council Bluff, monthly estimated correlations were 0.95, 0.78 and 0.80 with RMSE values of 20.56 $mmmon^{-1}$, 67.2 $mmmon^{-1}$ and 123.87 $mmmon^{-1}$ for CDR, CCS and PERSIANN, respectively. While annual estimated correlations were 0.95, 0.83 and 0.73 with RMSE values of 122.74 $mmyr^{-1}$, 475.06 $mmyr^{-1}$ and 704.4 $mmyr^{-1}$ for CDR, CCS and PERSIANN, respectively. For the Sheldon, monthly estimated correlations were 0.94, 0.63 and 0.72 with RMSE values of 22.59 $mmmon^{-1}$, 65.83 $mmmon^{-1}$ and 110.17 $mmmon^{-1}$ for CDR, CCS and PERSIANN, respectively. However, annual estimated correlations were 0.91, 0.42 and 0.31 with RMSE values of 171.12 $mmyr^{-1}$, 511.72 $mmyr^{-1}$ and 730.42 $mmyr^{-1}$ for CDR, CCS and PERSIANN datasets, respectively.

In the MRB, the GPPs were evaluated for the '432004' station and '431025' station which is located at an elevation of 126 m and 461 m, respectively. Meteorological data for both stations were available from 1993 to 2015. It was recognised that the GPPs had slightly overestimated the precipitation. For 432,004 station, monthly estimated correlations were 0.88, 0.74 and 0.73 with RMSE values of 57.96 $mmmon^{-1}$, 96.7 $mmmon^{-1}$ and 94.62 $mmmon^{-1}$ for CDR, CCS and PERSIANN, respectively. Likewise, annual estimated correlations were 0.49, 0.29 and 0.43 with RMSE values of 260.89 $mmyr^{-1}$, 430.43 $mmyr^{-1}$ and 410.00 $mmyr^{-1}$ for CDR, CCS and PERSIANN, respectively. For the 431,025 station, monthly estimated correlations were 0.85, 0.64 and 0.64 with RMSE values of 63.53 $mmmon^{-1}$, 100.73 $mmmon^{-1}$ and 95.38 $mmmon^{-1}$ for CDR, CCS and PERSIANN, respectively. However, annual estimated correlations were 0.62, 0.20 and 0.25 with RMSE values of 377.85 $mmyr^{-1}$, 523.85 $mmyr^{-1}$ and 452.25 $mmyr^{-1}$ for CDR, CCS and PERSIANN datasets, respectively.

Overall, among the three study basins, the most accurate GPPs estimates were observed in MLSB, USA followed by MRB, Thailand and lastly, BRB, Nepal. In terms of the precision and accuracy of the precipitation estimates from the precipitation products, regardless of the variation in temporal scale rainfall accumulation and neglecting the differences in altitude of the rainfall stations, it was revealed that PERSIANN accounted for the

largest errors in rainfall estimation in the BRB and MLSB while CCS had recorded the highest errors in rainfall estimation in the MRB. Despite these poor performances exhibited by both PERSIANN and CCS, the CDR had however demonstrated more significantly reliable rainfall estimates in all the study basins.

In general, all GPPs considered in this study tended to have a higher bias in high-altitude regions and this finding is somewhat consistent with the findings of Ombadi et al. [51]. Results obtained by the CDR estimates in the BRB were satisfactory and were aligned with the results obtained by Tan et al. [68] over the Tibetan Plateau, as correlation coefficient values between the range of 0.4 and 0.8 and RMSE values of large magnitude were parallelly obtained due to underestimations of rainfall estimates. Estimates of CDR in the MLSB were found to be the most accurate, as it exhibited the greatest correlations and least RMSE and is in the same context as mentioned by Ashouri et al. [5]. Moreover, the CDR estimates in the MRB performed averagely even though it had slightly overestimated as similarly found with the findings of Tang et al. [69]. Thus, based on these results, the CDR dataset was employed for further analysis in this study.

3.2. Trends of extreme precipitation indices

The extreme precipitation indices were developed for the period from 1993 to 2018. Initially, the precipitation indices were developed station-wise and the Thiessen polygon method was used for computing the mean precipitation indices for the catchments. Furthermore, their trends were computed at a confidence level of 95% using the XLSTAT package in Microsoft Excel.

In the BRB, CWD was the only extreme precipitation index that had a positive trend with a slope of 0.295 days/year, although it was not statistically significant. R10, R20, R35, R95p, R99p and PRCPTOT had statistically significant negative monotonic trends present. All indices, except CWD, showed very strong trends ($0 < p \leq 0.01$) while CWD showed a little trend ($0.1 < p \leq 0.5$). It was also observed that R10, R20 had considerable deviations to R35 although these indices had decreasing trends. It was quite alarming as R95p, R99p and PRCPTOT had very large negative slopes of −16.67 mm/year, −6.42 mm/year and − 18.69 mm/year, respectively.

In the MLSB, there were no monotonic trends were present. R10, R20, R35, R95p, R99p, PRCPTOT had increasing trends while CWD had a decreasing trend. The majority of the indices were found to have a little ($0.1 < p \leq 0.5$) to very little strength in their trends ($0.5 < p \leq 1.0$). R10 had a greater increasing trend in comparison to R20 and R35. The R95p, R99p and PRCPTOT had increasing trends and quite a similar Sen's slope. CWD was the only index that had a negative trend. However, it was very small and almost negligible as CWD had Kendall's tau and Sen's slope of −0.04 and − 0.01 days/year, respectively.

In the MRB basin, R35 and R99p had positive trends but were not statistically significant at a slope of 0.03 days/year and 0.328 mm/year, respectively. R35 had exhibited little strength in their trends while R99p had shown very little strength. While R10, R20, R95p, CWD, and PRCPTOT indicated negative trends with very little strength ($0.5 < p \leq 1.0$). R10 and R20 had negative trends at −0.014 days/year and − 0.05 days/year, respectively while R35 had a positive trend at 0.03 days/year. R95p had a negative trend at 0.64 mm/year while R99p indicated a positive trend at 0.33 mm/year. CWD and PRCPTOT too had negative trends at 0.01 days/year and − 0.9 mm/year, respectively. Table 3 depicts the summary of the trends in precipitation indices of the study basins. Fig. 6**.** illustrates the box and whisker plots for attributes and trends of the precipitation indices in the study basins. Refer to Supplementary Fig. S1-S3 for the illustration of the trends of the precipitation indices in the study basins.

Hence, the results of BRB were self-evident as it revealed that the number of days that received more than 10 mm, 20 mm and 35 mm daily rainfall amounts had significantly declined during the study period. In addition to this, declining trends were recorded for the annual total precipitation greater than the 95th and 99th percentiles of precipitation on wet days, which indicate that the rainfall received during the latter study period was significantly lesser than the during the beginning of the study period. Despite, these noteworthy decreases in rainfall patterns, it was also reported that the number of consecutively wet days had contrastingly increased. Taking everything into account, Tuladhar et al. [72] implied that most regions of the BRB received substantially lower rainfall from 2000 to 2015 and these findings were found to be quite consistent with the results of this study.

The MLSB had however experienced a higher number of days that received greater than 10 mm, 20 mm and 35 mm daily rainfall amounts. Moreover, the annual total precipitation greater than the 95th and 99th percentiles of precipitation on wet days had also shown an increment during the study period. But then again, it should be noted the fact that MLSB had comprised of the least mean among all indices in the three different study basins. However, these results have demonstrated homogeneity with the conclusions of Barbero et al. [7] and Sun et al. [67].

The MRB remarkably displayed a greater number of days that received greater than 35 mm daily rainfall amounts and also unveiled its growing trend of annual total precipitation greater than the 99th percentile of precipitation on wet days. In contrast, the number of days that received greater than 10 mm and 20 mm daily rainfall amounts have illustrated a decreasing trend. The obtained results showcased that the MRB had experienced spells of high-intensity rainfall events during the study period. The findings of Limsakul and Singhruck [43] and Sharma and Babel [59] are somewhat coherent with the findings of this study.

3.3. Historical land-use and land cover (LULC) change detection

LU change analysis was performed to assess the changes of each LU type from the remotely sensed data and GIS analysis of ESACCI-LC through the years of 1992 to 2015 of each basin. Each basin was projected to its specific UTM coordinate system before analyzing in ArcMap 10.1. Refer to Supplementary Table S2 for detailed attributes of land-use change in the study basins. Table 4 provides the percentage change per year of the land-use types of the selected study basins.

The BRB, Nepal has a total catchment area of 3420 km^2. This basin was projected into the WGS 84/UTM Zone 45 N for the analysis of LU change. The land-use types were classified into seven (7) major land-use types. In 1992, it was found that the BRB is dominated by forest cover (56.85%), followed by Cropland (19.85%), Natural Vegetation (17.93%), Urban built-up (2.90%), Grasslands (1.29%), Shrublands (0.95%) and Water

Table 3
Summary of precipitation indices in study Basins.

Indices	BRB, Nepal			MLSB, USA			MRB, Thailand		
	Kendall's Tau	Sen's Slope	*p*-value	Kendall's Tau	Sen's Slope	p-value	Kendall's Tau	Sen's Slope	p-value
R10 (days/year)	−0.33	−0.53	0.02	0.13	0.09	0.38	−0.03	−0.014	0.86
R20 (days/year)	−0.46	−0.49	0.001	0.03	0.02	0.86	−0.07	−0.05	0.63
R35 (days/year)	−0.44	−0.25	0.001	0.07	0.02	0.64	0.15	0.03	0.3
CWD (days/year)	0.22	0.26	0.124	−0.04	−0.01	0.81	−0.003	−0.01	1.0
R95p (mm/year)	−0.51	−16.7	0.0002	0.04	0.80	0.79	−0.05	−0.64	0.76
R99p (mm/year)	−0.53	−6.42	0.0002	0.10	0.95	0.49	0.05	0.33	0.73
PRCPTOT (mm/year)	−0.47	−18.7	0.001	0.02	0.78	0.93	−0.02	−0.90	0.90

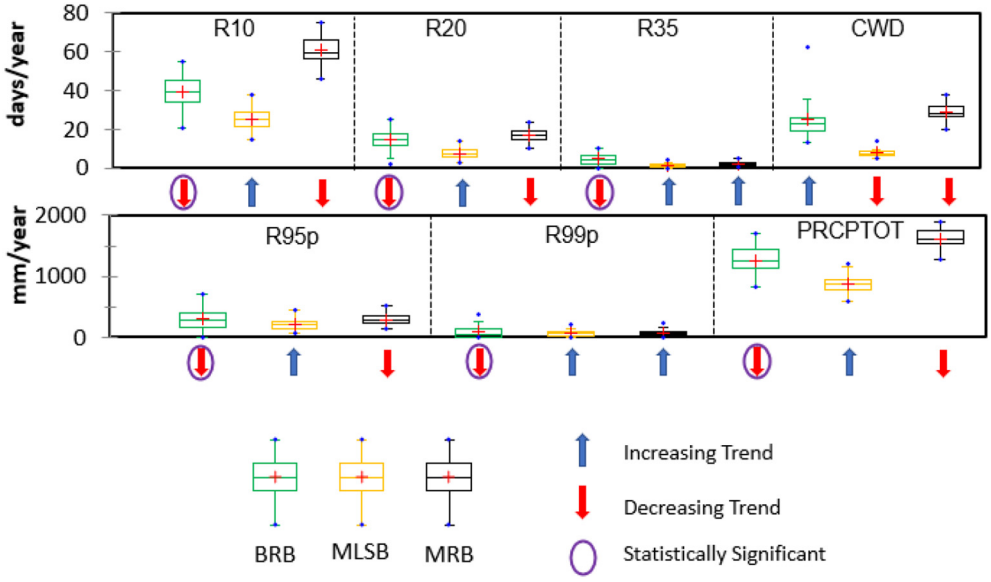

Fig. 6. Attributes of the Precipitation Indices in the Study Basins.

(0.23%). Urban built-up area in the BRB has expanded by 99.30 km^2, from 99.30 km^2 (2.90%) to 198.60 km^2 (5.81%) during 1992–2015 which is an overall roughly increase of 100% (4.17% change per year). The expansion in urban built-up areas has also resulted in the reduction of forest area by 6% (0.25% change per year) which accounts for an area of nearly 118 km^2. The results obtained on the expansion of urban built-up and decline of forest cover are well correlated with the findings of FAO [18] and Rijal et al. [57]. In addition to this, the shrubland area has reduced by 68% which can be expressed as a rate of change of 2.84% per year.

The MLSB, USA has a total catchment area of 24,248.22 km^2. This basin was projected into the WGS 84/UTM Zone 14 N for the analysis of LU change. The land-use types were classified into nine (9) major land-use types. In 1992, it was found that the MLSB is dominated by Cropland (87.09%), followed by Grasslands (6.58%), Natural Vegetation (2.60%), Forest (1.37%), Urban (1.21%), Wetlands (0.28%), Water (0.23%), Shrubland (0.07%) and Bare cover which is almost negligible (0.003%). It was observed that the cropland area has been reduced by approximately 186 km^2 (0.04% change per year) during the study period. Moreover, parallel findings were described by Jordan et al. [36] also stating specifically that the flood plain along the river channel exhibited a declining vegetation trend. In addition to this, the urban built-up area has expanded by nearly 165 km^2 (2.35% change per year), somewhat constant results were also revealed by Jordan et al. [36]. These results reveal that the natural infiltration capacity of the basin is affected and thereby increase the surface run-off of the basin. However, since there is an increment in forest cover, the interactions of the hydrological flow regime could be compromised to a certain extent.

The MRB, Thailand has a total surface area of 53,621 km^2. This basin was projected into the WGS 84/UTM Zone 47 N for the analysis of LU change. The land-use types were classified into eight (8) major land-use types. In 1992, it was found that the MRB basin is dominated by Cropland (69.94%), followed by Natural Vegetation (19.36%), Forest (6.63%), Shrubland (2.34%), Water (0.86%), Grasslands (0.73%), Urban (0.12%) and Wetland (0.02%). Overall, it was noticed that cropland, natural vegetation, forest, and grasslands have negative trends although they have increments in the middle of the time series. Shrublands, urban built-up, and water bodies have positive trends, with urban-built up taking 19.40% change per year which accounts for an expansion of 285.8 km^2. It was also observed that the forest cover had depreciated at a rate of 0.13% change per year which reduced the forest cover by 105.2 km^2. Wetlands had the least fluctuations throughout the period with an overall increment of 0.2 km^2. The land-use change results of this study were found to be somewhat steady with the discoveries of Yadav et al. [75], however, very few discrepancies were also observed which may have occurred due to the different sources of data and land-use classification schemes as suggested by Pérez-Hoyos et al. [54]. Fig. 7. depicts the spatial variation of land-use in the study basins from 1995 to 2015.

Table 4
Summary of land-use change in the study Basins.

	% change/year		
Land-use type	BRB, Nepal	MLSB, USA	MRB, Thailand
Cropland	0.17	−0.04	−0.02
Natural Vegetation	0.13	−0.03	–
Forest	−0.25	0.38	−0.13
Shrubland	−2.84	−0.68	0.13
Grasslands	−0.52	−0.01	−0.32
Wetlands	Not Present	0.06	0.07
Urban	4.17	2.35	19.40
Water	–	0.02	0.12

3.4. Identification of major flood cause

In the BRB, Nepal, a sample size of $n = 18$ (1993–2010) was used to analyze the contribution to APF of the BRB. For the land-use model, Forest, Urban, Cropland, Natural vegetation, and Grassland cover consisted of 99.47% of land cover types of the basin. Results showed that these predictor variables, explained a percentage contribution (R^2) of 16.4% on the dependant variable while it correlated 40.5% with the observed data. Results of the precipitation model showed that the precipitation variables can solely explain the contribution to APF by 40.8% in the BRB. The combined regression model had a Durbin-Watson value of 1.91 thus, indicating no autocorrelation among the variables. The combined model explained a percentage contribution (R^2) of 66.7% to the APF while it correlates 81.7% with the observed data.

In the MLSB, USA, a sample size of $n = 23$ (1993–2015) was used to analyze the contribution on APF of the MLSB. For the land-use model, predictor variables were Forest, Urban, Cropland and Natural vegetation cover consisted of 92.3% of land cover types of the basin. Results showed that these predictor variables explained a percentage contribution (R^2) of 21.8% to the APF while it correlates 46.7% with the recorded data. However, the results revealed via the precipitation model showed that the precipitation variables contributed 17.4% to the APF in the MLSB. The combined regression model had a Durbin-Watson value of 2.23 thus,

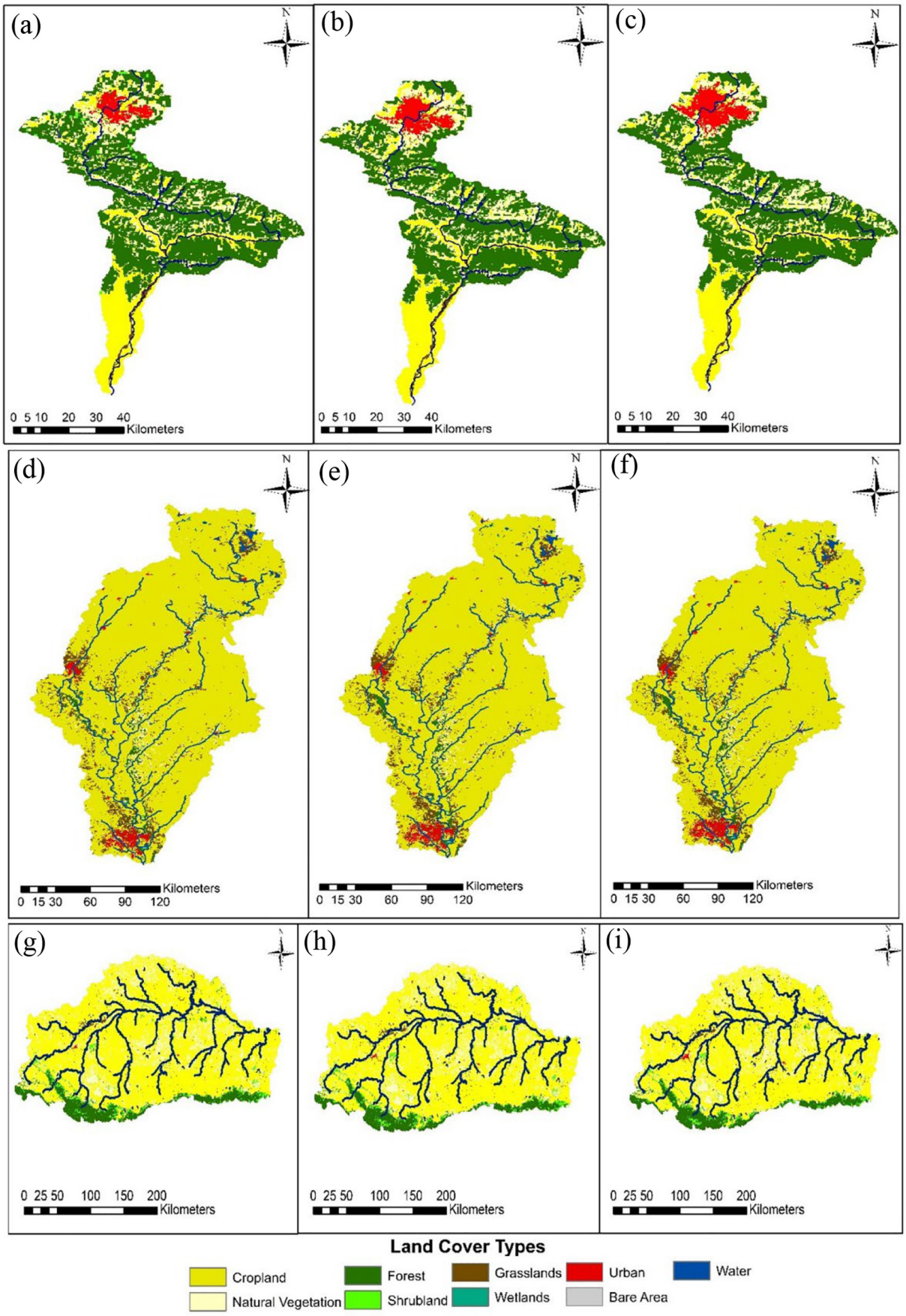

Fig. 7. LULC change in study Basins; Bagmati River Basin, Nepal (a) 1995 (b) 2005 (c) 2015, Missouri-Little Sioux Basin, USA (d) 1995 (e) 2005 (f) 2015, Mun River Basin, Thailand (g) 1995 (h) 2005 (i) 2015.

there was no autocorrelation among the variables. The combined regression model explained a percentage contribution (R^2) of 37.4% to the APF while it correlates 61.1% with the observed data.

In the MRB, Thailand, a sample size of $n = 20$ (1996–2015) was used to analyze the variations on the APF of the MRB. The land-use model used Cropland, Natural vegetation, Forest, Shrubland, Urban, Grassland cover which consisted of 99.1% of land cover types of the basin. Results showed that these variables explained a percentage contribution (R^2) of 27.7% on the dependant variable while it correlates 52.6% with observed data. For the precipitation model, the predictor variables explained a percentage contribution (R^2) of 57.3% to APF in MRB, Thailand. The combined regression model had a Durbin-Watson value of 2.52. The results of the overall model explained a percentage contribution (R^2) of 73.9% to the APF while it correlates 85.9% with the observed data. Refer to Supplementary Table S3-S5 for detailed contributions of the predictor variables in the study basin.

In general, the outcome of the resultant statistical models in each basin was satisfactory when compared with the findings of Bradshaw et al. [10] that accounted for 65% of the contribution to the flood, of which 14% were forest cover variables alone. In the BRB, the combined predictor variables demonstrated that 66.7% of the contribution to the flood has been due to the inclusion of these variables. However, the major flood attribute among the major predictors was extreme precipitation, as these variables collectively accounted for 40.8%. The LULC predictors however contributed 16.4% to the flooding of which 12.7% accounted for the cropland. This is since cropland regions are constantly under immense grazing pressure in addition to the rigorous annual cropping which has been proved by Costa et al. [14] that it affects the natural hydrological flow regime. In contrast, Dhital and Kayastha [16] understood that increases in the probability of flooding even for moderate rainfall events are due to the vast gradient changes in the Bagmati river that causes very high velocities in the river flow in the uplands, that lead to sediment deposition in the lowlands which raises the riverbed level which in turn makes a small flood more likely to topple the river and exacerbates the exposure and vulnerability of the residents in the lowlands.

In the MLSB, the combined predictor variables exhibited a total contribution of 37.4% to the flood. Unlike in the BRB, the major flood attribute in the MLSB among the major predictors was found to be LULC, as its contribution of 21.8% was greater than the precipitation which accounted for 17.4%. This reveals that more than 60% of unknown potential factors were likely to contribute to the flood in MLSB. The majority of the LULC contribution was a resultant due to the urban expansion in the watershed, hence, contributing the majority of 8.8%. In terms of the contribution from precipitation, it was reported that the majority of the contribution to the flood was as an impact due to the consecutive wet days which had attributed 9.5% of the total precipitation contribution. The results of this basin are well supported with the findings of Onsrud et al. [53] as they stated the basin has experienced gradual suburbanization, more channelization and less rangeland due to intensive annual cropping given the circumstance that the watershed is dominated by cropland cover. Moreover, the flooding event took place in Mid-March which denotes the conclusion of the winter term and the inception of spring. As a result, the rise in ambient air temperature, the snowmelt, together with the precipitation and icy soils are likely to generate substantial flooding of main rivers during this period which is also supported by the insights of Hillaker [27].

The highest contribution from the combined predictor variables among the study basins was observed in MRB, revealing a total contribution of 73.9% to the flooding. As in the case of BRB, the major flood attribute in the MRB was the extreme precipitation, accounting for 57.3% while the LULC had contributed 27.7%. In terms of the contribution from LULC, it was found that the majority of the attributes were due to reductions in grassland and forest cover in the MRB which contributed 16.3% and 6.5%, respectively. It is also noteworthy, that MRB accounted for the highest rate of change of urbanization, however, its contribution to the flood was less than 1%. About contribution from precipitation, it was noted that the annual wet day precipitation accounted for 30.5% of the contribution of extreme precipitation which was found to be statistically significant. In addition to this, the views of Prabnakorn et al. [55] are adjacent with the study findings, as they mentioned that the upstream river is complex and meandering that forms natural barriers to obstruct the water flow, encouraging higher water-levels, and increases the probability of flooding during the wet months (August to October). Refer to Table 5 for the summary of the tabulated results in the study basins.

Table 5
Summary of regression results in study basins.

Basin	Coefficient of Determination (R^2)			Major Flood Cause
	Land-use	Precipitation	Land-use + Precipitation	
BRB, Nepal	16.4%	40.8%	66.7%	Precipitation
MLSB, USA	21.8%	17.4%	37.4%	Land-use
MRB, Thailand	27.7%	57.3%	73.9%	Precipitation

Overall, this study mainly focussed on utilizing global datasets to identify the major flood attribute among LU change (due to the impacts of urbanization and deforestation) and heavy precipitation (due to human-induced climate change) in the three geographically-independent river basins. As the results suggest, these global datasets are capable of exhibiting robust performances for both precipitation and LULC as the results are well aligned with past studies. Yet again, these datasets comprise issues concerning data quality, the extent of coverage and spatial resolution due to inactive geostationary satellites and the number of input sensors (multi-sensors) used which directly affects the standard of the quality of the data acquired [26]. Apart from LULC and precipitation, it should be mentioned that other potential factors can be apprehended as flood attributes. Few other potential factors could be, poor waste management which could affect the natural drainage and mismanagement of surface water [71], ineffective urban planning and increased urban imperviousness which affects stormwater management [4,58], failure of water-retaining structures, topographical and geomorphological features which effects on the surface runoff and infiltration capacity [15,74] and thermal effects on micro-climatic changes [35].

4. Conclusion

This study demonstrates the application of the global dataset products in 3 independent climatic regions where this study aims at investigating the major attribute for flooding in the selected basins. This study evaluated the PERSIANN precipitation products together with the application of the ESACCI-LC dataset on the BRB, Nepal, MLSB, the United States and the MRB, Thailand. The reliability of the estimates of the GPPs was validated with observed rain-gauge records using statistical indicators. The results depicted that CDR estimates were accurate than the estimates of CCS and PERSIANN in the selected study basins. This was noteworthy, as generally, the finer resolution data have proven to provide the most accurate data. However, the findings of this study suggest that the coarser-resolution data exhibited higher accuracy and reliability than the finer resolution data illustrating that the accuracy depends mainly on the sources of data retrieval, satellite algorithms/data assimilation schemes utilized and the number of input sensors put to use. Thus, utilizing the CDR dataset as a successor, further analysis was conducted by the development of extreme precipitation indices and their trends.

Furthermore, all the study basins were impacted by urbanization with the MRB being struck to the greatest extent. Likewise, the MRB and the BRB were highly impacted by deforestation, unlike MLSB which had a fluctuating forest trend during the study period. Finally, by establishing a statistical relationship between the flood and the precipitation and land-use variables using the Multiple Linear Regression technique, the results demonstrated that the land-use change was the major cause for flooding in the MLSB while the root cause for flooding in the BRB and MRB was as a result of extreme precipitation trends.

Estimates of CDR can be effectively used by researchers and practitioners that lack precipitation data in ungauged areas of tropical and

temperate regions as it produced the most reliable estimates in comparison to the other considered GPP products. In addition to this, the results of ESACCI-LC data were found alike with previous research findings revealing that this LULC data can be employed to conduct LULC change analysis effectively. Moreover, the utilization of the CCS product can be used to monitor storm developments in the study basins as it has good detection capabilities and can be implemented as a decision-making tool for real-time flood warning systems. Furthermore, the developed statistical model can be more effectively applied and replicated in regions with tropical and sub-tropical climates. Hence, the application of this statistical model would assist researchers as well as relevant stakeholders such as urban development departments, disaster management and mitigation centres, etc. in identifying the major flood attribute of the river basins to develop the required flood-control measures, flood planning, land-use policies, and management to mitigate the damages in response to future flood events. Hence, reducing the exposure and vulnerability of the people and property and in turn raising the resiliency.

The variability in elevation played a pivotal role in the biases of all GPPs thus, the precipitation estimates may be enhanced via algorithm corrections for elevation, incorporation of multi-satellite passive microwave data and gauge calibration of the GPPs. Moreover, it is recommended that more GPPs could be evaluated for their reliability in the study basins such that it would improve the accuracy of the results. In terms of the statistical model, involving geomorphologic, drainage and temperature variables could improve model results as these features possess the potential for flooding in temperate regions. Additionally, applications of hydraulic and hydrological modelling may perhaps be incorporated together with flood-risk mapping which may be applied as a tool to identify the flood-prone regions such that the relevant communities are well informed on their vulnerability as well as their exposure to future floods.

Author statement

The first author collected data, conducted modelling experiments. The second author conceptualized the research. All other authors contributed in terms of comments and suggestions to improve the research.

Declaration of Competing Interest

The authors declare that they have no known competing financial interests or personal relationships that could have appeared to influence the work reported in this paper.

Acknowledgements

The authors gratefully acknowledge the Center for Hydrometeorology and Remote Sensing (CHRS) at the University of California, Irvine (UCI), Department of Hydrology and Meteorology (DHM), Nepal, Royal Thai Meteorological Department (TMD), Royal Thai Irrigation Department (RID), GRDC/German Federal Institute of Hydrology (BfG), ESA CCI Land Cover Project and the Dartmouth Flood Observatory (DFO) for generously providing data and time.

Appendix A. Supplementary data

Supplementary data to this article can be found online at https://doi.org/10.1016/j.pdisas.2021.100212.

References

[1] Adler RF, Huffman GJ, Chang A, Ferraro R, Xie PP, Janowiak J, et al. The version-2 global precipitation climatology project (GPCP) monthly precipitation analysis (1979-present). J Hydrometeorol. 2003;4(6):1147–67. https://doi.org/10.1175/1525-7541(2003)004<1147:TVGPCP>2.0.CO;2.

[2] AghaKouchak A, Nakhjiri N. A near real-time satellite-based global drought climate data record. Environ Res Lett. 2012;7(4):44037.

[3] Alexakis DD, Grillakis MG, Koutroulis AG, Agapiou A, Themistocleous K, Tsanis IK, et al. GIS and remote sensing techniques for the assessment of land-use change impact on flood hydrology: the case study of Yialias basin in Cyprus. Nat Hazards Earth Syst Sci. 2014;14(2):413–26. https://doi.org/10.5194/nhess-14-413-2014.

[4] Amoako C, Boamah EF. The three-dimensional causes of flooding in Accra, Ghana. Int J Urban Sustain Develop. 2015;7(1):109–29. https://doi.org/10.1080/19463138.2014.984720.

[5] Ashouri H, Hsu KL, Sorooshian S, Braithwaite DK, Knapp KR, Cecil LD, et al. PERSIANN-CDR: daily precipitation climate data record from multisatellite observations for hydrological and climate studies. Bull Am Meteorol Soc. 2015;96(1):69–83. https://doi.org/10.1175/BAMS-D-13-00068.1.

[6] Babel MS, Bhusal SP, Wahid SM, Agarwal A. Climate change and water resources in the Bagmati River basin, Nepal. Theor Appl Climatol. 2014;115(3–4):639–54. https://doi.org/10.1007/s00704-013-0910-4.

[7] Barbero R, Fowler HJ, Lenderink G, Blenkinsop S. Is the intensification of precipitation extremes with global warming better detected at hourly than daily resolutions? Geophys Res Lett. 2017;44(2):974–83.

[8] Bartholome E, Belward AS. GLC2000: a new approach to global land cover mapping from earth observation data. Int J Remote Sens. 2005;26(9):1959–77. https://doi.org/10.1080/01431160412331291297.

[9] Behrangi A, Khakbaz B, Jaw TC, AghaKouchak A, Hsu K, Sorooshian S. Hydrologic evaluation of satellite precipitation products over a mid-size basin. J Hydrol. 2011;397(3–4):225–37. https://doi.org/10.1016/j.jhydrol.2010.11.043.

[10] Bradshaw CJA, Sodhi NS, Peh KSH, Brook BW. Global evidence that deforestation amplifies flood risk and severity in the developing world. Glob Chang Biol. 2007;13(11):2379–95. https://doi.org/10.1111/j.1365-2486.2007.01446.x.

[11] Chen Y. Spatial autocorrelation approaches to testing residuals from least squares regression. PLoS One. 2016.;11(1):e0146865. https://doi.org/10.1371/journal.pone.0146865.

[12] Chirachawala C, Shrestha S, Babel MS, Virdis SG, Wichakul S. Evaluation of global land use/land cover products for hydrologic simulation in the upper Yom River basin, Thailand. Sci Total Environ. 2020.;708:135148. https://doi.org/10.1016/j.scitotenv.2019.135148.

[13] Contreras J, Mendoza D, Pacheco J, Avilés A. The influence of global climate and local hydrological variations over streamflow extremes: the tropical-mountain case. Hydrol Earth Syst Sci Discuss. 2019.;1–37. https://doi.org/10.5194/hess-2019-554.

[14] Costa MH, Botta A, Cardille JA. Effects of large-scale changes in land cover on the discharge of the Tocantins River, southeastern Amazonia. J Hydrol. 2003;283(1–4):206–17. https://doi.org/10.1016/S0022-1694(03)00267-1.

[15] Dalu MTB, Shackleton CM, Dalu T. Influence of land cover, proximity to streams and household topographical location on flooding impact in informal settlements in the eastern cape, South Africa. Int J Disaster Risk Reduct. 2018;28:481–90. https://doi.org/10.1016/j.ijdrr.2017.12.009.

[16] Dhital YP, Kayastha RB. Frequency analysis, causes and impacts of flooding in the Bagmati River basin, Nepal. J Flood Risk Manage. 2013;6(3):253–60. https://doi.org/10.1111/jfr3.12013.

[17] ESA. Land cover CCI product user guide version 2. Tech Rep. 2017. Available at: maps.elie.ucl.ac.be/CCI/viewer/download/ESACCI-LC-Ph2-PUGv2_2.0.pdf.

[18] FAO. Global forest resource assessment 2005. Rome, Italy: Food and Agriculture Organization of the United Nations; 2006; 27–30.

[19] Ferreira S, Ghimire R. Forest cover, socioeconomics, and reported flood frequency in developing countries. Water Resour Res. 2012.;48(8). https://doi.org/10.1029/2011WR011701.

[20] FloodList. Updated_ Nepal – Dozens Dead After Heavy Monsoon Rains – FloodList. http://floodlist.com/asia/nepal-monsoon-floods-july-2019; 2019.

[21] FloodList. USA – 3 Dead as Rivers Reach Record Highs in Iowa and Nebraska – FloodList. http://floodlist.com/america/usa/iowa-nebraska-floods-march-2019; 2019.

[22] Friedl MA, Sulla-Menashe D, Tan B, Schneider A, Ramankutty N, Sibley A, et al. MODIS collection 5 global land cover: algorithm refinements and characterization of new datasets. Remote Sens Environ. 2010;114(1):168–82. https://doi.org/10.1016/j.rse.2009.08.016.

[23] Gado TA, Hsu K, Sorooshian S. Rainfall frequency analysis for ungauged sites using satellite precipitation products. J Hydrol. 2017;554:646–55.

[24] Glen S. Durbin Watson Test & Test Statistic. https://www.statisticshowto.com/durbin-watson-test-coefficient/; 2016.

[25] Guha-Sapir D, Vos F, Below R, Ponserre S. Annual Disaster Statistical Review 2011: The Numbers and Trends; 2012.

[26] Gunathilake MB, Amaratunga YV, Perera A, Karunanayake C, Gunathilake AS, Rathnayake U. Statistical evaluation and hydrologic simulation capacity of different satellite-based precipitation products (SbPPs) in the upper Nan River basin, northern Thailand. J Hydrol: Region Stud. 2020.;32:100743. https://doi.org/10.1016/j.ejrh.2020.100743.

[27] Hillaker H. The Precipitation Climatology of Iowa. https://media.cocorahs.org/docs/ClimateSum_IA.pdf; 2019.

[28] Hong H, Panahi M, Shirzadi A, Ma T, Liu J, Zhu AX, et al. Flood susceptibility assessment in Hengfeng area coupling adaptive neuro-fuzzy inference system with genetic algorithm and differential evolution. Sci Total Environ. 2018;621:1124–41. https://doi.org/10.1016/j.scitotenv.2017.10.114.

[29] Hong Y, Hsu K-L, Sorooshian S, Gao X. Precipitation estimation from remotely sensed imagery using an artificial neural network cloud classification system. J Appl Meteorol. 2004;43(12):1834–53. https://doi.org/10.1175/JAM2173.1.

[30] Hsu, K. L., Sellars, S., Nguyen, P., Braithwaite, D., Chu, W., & others. (2013). G-WADI PERSIANN-CCS GeoServer for extreme precipitation event monitoring. Sci Cold Arid Regions, 5(1), 6–15.

[31] Hsu K-L, Hong Y, Sorooshian S. Rainfall estimation using a cloud patch classification map. Measuring precipitation from space. Springer; 2007. p. 329–42.

[32] Hsu Kou-lin, Gao X, Sorooshian S, Gupta HV. Precipitation estimation from remotely sensed information using artificial neural networks. J Appl Meteorol. 1997;36(9):1176–90.
[33] Hsu Kuo-lin, Gupta HV, Gao X, Sorooshian S. Estimation of physical variables from multichannel remotely sensed imagery using a neural network: application to rainfall estimation. Water Resour Res. 1999;35(5):1605–18.
[34] Huffman GJ, Bolvin DT, Nelkin EJ, Wolff DB, Adler RF, Gu G, et al. The TRMM multisatellite precipitation analysis (TMPA): quasi-global, multiyear, combined-sensor precipitation estimates at fine scales. J Hydrometeorol. 2007;8(1):38–55. https://doi.org/10.1175/JHM560.1.
[35] Huong HTL, Pathirana A. Urbanization and climate change impacts on future urban flooding in Can Tho city, Vietnam. Hydrol Earth Syst Sci. 2013;17(1):379–94.
[36] Jordan YC, Ghulam A, Herrmann RB. Floodplain ecosystem response to climate variability and land-cover and land-use change in lower Missouri River basin. Landsc Ecol. 2012;27(6):843–57.
[37] Juglea S, Kerr Y, Mialon A, Lopez-Baeza E, Braithwaite D, Hsu K. Soil moisture modelling of a SMOS pixel: interest of using the PERSIANN database over the Valencia Anchor Station. Hydrol Earth Syst Sci. 2010;14(8):1509–25.
[38] Katiraie-Boroujerdy P-S, Nasrollahi N, Hsu K, Sorooshian S. Evaluation of satellite-based precipitation estimation over Iran. J Arid Environ. 2013;97:205–19.
[39] Khan SI, Adhikari P, Hong Y, Vergara H, Adler RF, Policelli F, et al. Hydroclimatology of Lake Victoria region using hydrologic model and satellite remote sensing data. Hydrol Earth Syst Sci. 2011;15(1):107–17. https://doi.org/10.5194/hess-15-107-2011.
[40] Khattak MS, Babel MS, Sharif M. Hydro-meteorological trends in the upper Indus River basin in Pakistan. Clim Res. 2011;46(2):103–19. https://doi.org/10.3354/cr00957.
[41] Khosravi K, Nohani E, Maroufinia E, Pourghasemi HR. A GIS-based flood susceptibility assessment and its mapping in Iran: a comparison between frequency ratio and weights-of-evidence bivariate statistical models with multi-criteria decision-making technique. Nat Hazards. 2016;83(2):947–87. https://doi.org/10.1007/s11069-016-2357-2.
[42] Kutner MH, Nachtsheim CJ, Neter J, Li W, et al. Applied linear statistical models. , vol. 5McGraw-Hill Irwin New York; 2005..
[43] Limsakul A, Singhruck P. Long-term trends and variability of total and extreme precipitation in Thailand. Atmos Res. 2016;169:301–17.
[45] Mehran A, AghaKouchak A. Capabilities of satellite precipitation datasets to estimate heavy precipitation rates at different temporal accumulations. Hydrol Process. 2014;28(4):2262–70.
[46] Messner F, Meyer V. Flood damage, vulnerability and risk perception – Challenges for flood damage research. Flood risk management: Hazards, vulnerability and mitigation measures. Netherlands: Springer; 2006. p. 149–67. https://doi.org/10.1007/978-1-4020-4598-1_13.
[47] Miao C, Ashouri H, Hsu K-L, Sorooshian S, Duan Q. Evaluation of the PERSIANN-CDR daily rainfall estimates in capturing the behavior of extreme precipitation events over China. J Hydrometeorol. 2015;16(3):1387–96.
[48] Mousivand A, Arsanjani JJ. Insights on the historical and emerging global land cover changes: the case of ESA-CCI-LC datasets. Appl Geogr. 2019;106:82–92. https://doi.org/10.1016/j.apgeog.2019.03.010.
[49] Nguyen P, Thorstensen A, Sorooshian S, Zhu Q, Tran H, Ashouri H, et al. Evaluation of CMIP5 model precipitation using PERSIANN-CDR. J Hydrometeorol. 2017;18(9):2313–30.
[50] Nguyen P, Ombadi M, Sorooshian S, Hsu K, AghaKouchak A, Braithwaite D, et al. The PERSIANN family of global satellite precipitation data: a review and evaluation of products. Hydrol Earth Syst Sci. 2018;22(11):5801–16.
[51] Ombadi M, Nguyen P, Sorooshian S, Hsu K, lin. Developing intensity-duration-frequency (IDF) curves from satellite-based precipitation: methodology and evaluation. Water Resour Res. 2018;54(10):7752–66. https://doi.org/10.1029/2018WR022929.
[52] Ongsomwang S, Pukongduean P. Urban flood mitigation and prevention using the Mike 21 model: a case study of Nakhon Ratchasima Province, Thailand. Suranaree J Sci Technol. 2016. ;23(4).
[53] Onsrud A, Richter D, Chirhart J, Koschak M, Christopherson D, Duffey D, et al. Missouri River Basin (Upper Big Sioux, Lower Big Sioux, Little Sioux, and Rock River watersheds) monitoring and assessment report. September, 293. http://www.pca.state.mn.us/index.php/view-document.html?gid=21888; 2014.
[54] Pérez-Hoyos A, Rembold F, Kerdiles H, Gallego J. Comparison of global land cover datasets for cropland monitoring. Remote Sens. 2017;9(11):1118. https://doi.org/10.3390/rs9111118.
[55] Prabnakorn S, Suryadi FX, Chongwilaikasem J, De Fraiture C. Development of an integrated flood hazard assessment model for a complex river system: a case study of the Mun River basin, Thailand. Model Earth Syst Environ. 2019;5(4):1265–81.
[56] Pradhan B. Flood susceptible mapping and risk area delineation using logistic regression, GIS and remote sensing. J Spat Hydrol. 2009;9(2):1–18.
[57] Rijal S, Rimal B, Acharya RP, Stork NE. Land use/land cover change and ecosystem services in the Bagmati River basin, Nepal. Environ Monit Assess. 2021;193(10):1–17.
[58] KC S, Shrestha S, Ninsawat S, Chonwattana S. Predicting flood events in Kathmandu Metropolitan City under climate change and urbanisation. J Environ Manag. 2021.; 281:111894. https://doi.org/10.1016/j.jenvman.2020.111894.
[59] Sharma D, Babel MS. Trends in extreme rainfall and temperature indices in the western Thailand. Int J Climatol. 2014;34(7):2393–407.
[60] Shrestha S, Gyawali B, Bhattarai U. Impacts of climate change on irrigation water requirements for rice-wheat cultivation in Bagmati River basin, Nepal. J Water Clim Change. 2013;4(4):422–39. https://doi.org/10.2166/wcc.2013.050.
[61] Smith TM, Arkin PA, Bates JJ, Huffman GJ. Estimating Bias of satellite-based precipitation estimates. J Hydrometeorol. 2006;7(5):841–56. https://doi.org/10.1175/JHM524.1.
[62] Sorooshian S, Hsu KL, Gao X, Gupta HV, Imam B, Braithwaite D. Evaluation of PERSIANN system satellite-based estimates of tropical rainfall. Bull Am Meteorol Soc. 2000;81(9):2035–46. https://doi.org/10.1175/1520-0477(2000)081<2035:EOPSSE>2.3.CO;2.
[63] Sorooshian S, Gao X, Hsu K, Maddox RA, Hong Y, Gupta HV, et al. Diurnal variability of tropical rainfall retrieved from combined GOES and TRMM satellite information. J Clim. 2002;15(9):983–1001.
[64] Stewart B. Measuring what we manage - the importance of hydrological data to water resources management. IAHS-AISH Proceed Reports. 2015;366:80–5.
[65] Subramanya K. Engineering hydrology. 4e. Tata McGraw-Hill Education; 2013..
[66] Sun Q, Miao C, Duan Q, Ashouri H, Sorooshian S, Hsu KL. A review of global precipitation data sets: data sources, estimation, and Intercomparisons. Rev Geophys. 2018;56(1):79–107. https://doi.org/10.1002/2017RG000574.
[67] Sun Q, Zhang X, Zwiers F, Westra S, Alexander LV. A global, continental, and regional analysis of changes in extreme precipitation. J Clim. 2021;34(1):243–58.
[68] Tan X, Ma Z, He K, Han X, Ji Q, He Y. Evaluations on gridded precipitation products spanning more than half a century over the Tibetan plateau and its surroundings. J Hydrol. 2020.;582:124455. https://doi.org/10.1016/j.jhydrol.2019.124455.
[69] Tang X, Zhang J, Gao C, Ruben GB, Wang G. Assessing the uncertainties of four precipitation products for swat modeling in Mekong River basin. Remote Sens. 2019;11(3):304. https://doi.org/10.3390/rs11030304.
[70] The International Water Association. Flood control and disaster management. IWA Publishing; 2013. https://www.iwapublishing.com/news/flood-control-and-disaster-management.
[71] The World Bank. Leveraging urbanization in Bangladesh. World Bank; 2015. https://www.worldbank.org/en/country/bangladesh/brief/leveraging-urbanization-bangladesh.
[72] Tuladhar D, Dewan A, Kuhn M, Corner RJ. Spatio-temporal rainfall variability in the Himalayan mountain catchment of the Bagmati River in Nepal. Theor Appl Climatol. 2020;139(1):599–614. https://doi.org/10.1007/s00704-019-02985-8.
[73] VanVoorhis CW, Morgan BL. Understanding power and rules of thumb for determining sample sizes. Tutor Quant Methods Psychol. 2007;3(2):43–50. https://doi.org/10.20982/tqmp.03.2.p043.
[74] Westra S, Fowler HJ, Evans JP, Alexander LV, Berg P, Johnson F, et al. Future changes to the intensity and frequency of short-duration extreme rainfall. Rev Geophys. 2014;52(3):522–55. https://doi.org/10.1002/2014RG000464.
[75] Yadav S, Babel MS, Shrestha S, Deb P. Land use impact on the water quality of large tropical river: Mun River basin, Thailand. Environ Monit Assess. 2019;191(10):1–22. https://doi.org/10.1007/s10661-019-7779-3.
[76] Yilmaz KK, Hogue TS, Hsu K, Sorooshian S, Gupta HV, Wagener T. Intercomparison of rain gauge, radar, and satellite-based precipitation estimates with emphasis on hydrologic forecasting. J Hydrometeorol. 2005;6(4):497–517.
[77] Zhang X, Yang F. RClimDex (1.0) user manual. Clim Res Branch Environ Canada. 2004. ; 22.
[78] Ziese M, Rauthe-Schöch A, Becker A, Finger P, Meyer-Christoffer A, Schneider U. GPCC full data daily version. 2018 at 1.0: daily land-surface precipitation from rain-gauges built on GTS-based and historic data; 2018..
[79] Mann HB. Nonparametric tests against trend. Econometrica: Journal of the Econometric Society. 1945:245–59.
[80] Sen PK. Estimates of the regression coefficient based on Kendall's tau. Journal of the American Statistical Association. 1968;63(324):1379–89.